Nonlinear concentration patterns and bands in autochemotactic suspensions

Enkeleida Lushi,[1] Raymond E. Goldstein,[2] and Michael J. Shelley[3,4]

[1]*Department of Mathematics, New Jersey Institute of Technology, Newark, New Jersey 07102, USA*
[2]*Department of Applied Mathematics and Theoretical Physics, University of Cambridge, Cambridge CB3 0WA, United Kingdom*
[3]*Center for Computational Biology, Flatiron Institute, Simons Foundation, New York, New York 10010, USA*
[4]*Courant Institute of Mathematical Sciences, New York University, New York, New York 10012, USA*

In suspensions of microorganisms, pattern formation can arise from the interplay of chemotaxis and the fluid flows collectively generated by the organisms themselves. Here we investigate the resulting pattern formation in square and elongated domains in the context of two distinct models of locomotion in which the chemoattractant dynamics is fully coupled to the fluid flows and swimmer motion. Analyses for both models reveal an aggregative instability due to chemotaxis, independent of swimmer shape and type, and a hydrodynamic instability for "pusher" swimmers. We discuss the similarities and differences between the models. Simulations reveal a critical length scale of the swimmer aggregates and this feature can be utilized to stabilize swimmer concentration patterns into quasi-one-dimensional bands by varying the domain size. These concentration bands transition to traveling pulses under an external chemoattractant gradient, as observed in experiments with chemotactic bacteria.

I. INTRODUCTION

Recent advances in experiments and in theoretical modeling have established that suspensions of motile microorganisms can organize into complex patterns and collectively generate significant fluid flows (e.g., Refs. [1–11]). These large-scale patterns can occur in the bulk in the absence of directional cues for swimming and are mediated by steric and hydrodynamic interactions between the microswimmers [12,13]. It is also well known that motile microorganisms can exhibit directed chemotactic motions in response to chemical cues in their environment. When those cues are attractive and produced by the motile organisms themselves, then collective aggregation can occur. We refer to such a situation as "autochemotactic" in that the colony is responding to its own self-generated signals. However, many of the classical experiments on autochemotactic aggregation, which can show intricate patterns such as bands and arrays of spots, were performed in environments where hydrodynamic coupling between the motile cells is not expected to be strong (e.g., in the thin fluid layer atop an agar plate [14,15]). Chemotactic systems are considerably more complicated when the constituent organisms are moving in an open fluid and can generate flows, since these flows will also advect the chemoattractant. These collectively generated flows can affect chemotactic aggregation and patterning of microorganisms and possibly affect the modes of colonial communication such as through quorum sensing [16,17]. Here we investigate these issues in the context of two theoretical models that combine the fluid flows generated by a motile suspension with the production, advection, and diffusion of a swimmer-generated chemoattractant and the response of the swimmers to this chemoattractant field.

Pattern formation through chemotactic aggregation has been studied extensively since the pioneering theoretical work on the Keller-Segel (KS) model [18,19] and its many variants. The KS model couples evolution of a cell concentration field to an intrinsically generated, diffusing chemoattractant field. In its simplest form, where the cell velocity scales linearly with chemoattractant gradient, the KS model can lead to infinite concentrations in finite time [20]. In most models such behavior is typically avoided through the inclusion of *ad hoc* saturation terms [21]. Kinetic theories have been developed for the dynamics of bacterial populations in which the individual organisms execute modulated run-and-tumble motions in response to a chemoattractant gradient [21–28]. In these models, tumbling frequency decreases (and run length increases) if the organism moves up the attractant gradient, as is observed experimentally [29,30].

Our previous study [31] considered the effects of the collectively generated fluid flows on the chemotactic aggregation of run-and-tumble swimmers. These fluid flows advect chemoattractants and perturb the motions of the constituent swimmers and were found to affect the overall dynamics. We also found that accounting for the fluid dynamics may remove the need for *ad hoc* saturation terms used in some chemotaxis models as the fluid flows inhibit unphysical concentration blow-ups. We revisit and explore further microswimmer chemotactic dynamics that includes the effect of the self-generated fluid flows. We make use of two kinetic models. The first we consider is a run-and-tumble one based on the biased random walk exhibited by bacteria, the very same we introduced in Ref. [31]. As an interesting alternative we also present a second model in which swimmers perform chemotaxis by directly detecting spatial chemoattractant gradients and responding to them by rotating in the direction of the chemoattractant gradient. This type of model is more appropriate for larger eukaryotic microswimmers such as spermatozoa and nontumbling microswimmers. Merging these

chemotaxis models with the active suspension model is seamless as both these models are kinetic theories with particle position and orientation as their conformation variables [31,32].

For both models, linear stability analysis of isotropic swimmer suspensions yields two separate branches of instability: one associated with chemotaxis-driven aggregation and the other a "hydrodynamic" instability that drives swimmer alignment through the development of large-scale fluid flows associated with "pusher" suspensions. The fully coupled nonlinear systems studied through simulations reveal that swimmer generated fluid flows can have a significant effect on aggregation dynamics. Remarkably, despite differences to the run-and-tumble chemotaxis model, the "turning-particle" chemotaxis model exhibits many of the same dynamical features in the long wave regimes when the parameters are matched as suggested by linear analysis. For regimes far from the hydrodynamic instability, we find that neutral swimmer and puller aggregates to become stable, circular, and saturated, whereas pusher aggregates become elongated and can move due to local straining fluid flows. The critical size of these aggregates can be predicted by linear analysis. We find that when the suspension is confined in narrow domains with a width below the critical length scale predicted by analysis, these aggregates transition into quasi-one-dimensional bands. Moreover, when subjected to a constant external chemoattractant gradient, these bands travel in that direction and develop profiles reminiscent to those seen in experiments with chemotactic *Escherichia coli* in microchannels [26]. This works suggests that these continuum models can be appropriately modified to study other chemotactic phenomena.

II. MATHEMATICAL MODEL

A. The run-and-tumble model

We first review the recent model developed in Ref. [31], which incorporates a *run and tumble* (RT) chemotactic response into a kinetic theory of motile suspensions. Bacteria such as *E. coli* typically perform a biased random walk which enables them to move up chemoattractant gradients [30]. Such a random walk consists of a series of runs and tumbles whose frequency decreases when a bacterium is moving in a favorable direction of increasing chemoattractant concentration. This RT chemotaxis model is based on Alt's formulation [22] and extends subsequent models [23,24,33].

Consider self-propelled ellipsoidal-shaped swimmers each moving with constant speed $U_0 := 1$ in a fluid. The swimmer center-of-mass is denoted by $\mathbf{x}$ and its swimming direction along its main axis is $\mathbf{p}$ ($|\mathbf{p}| = 1$). The configuration of microswimmers is given by a distribution function $\Psi(\mathbf{x}, \mathbf{p}, t)$. The positional and orientational dynamics of a suspension of swimmers that individually execute run-and-tumbles is described by a Fokker-Planck equation for conservation of microswimmer number:

$$\frac{\partial \Psi}{\partial t} = -\nabla_x \cdot [\Psi \dot{\mathbf{x}}] - \nabla_p \cdot [\Psi \dot{\mathbf{p}}]$$
$$- \left[\Psi \lambda(\mathcal{D}_t C) - \frac{1}{4\pi} \int \Psi(\mathbf{p}') \lambda(\mathcal{D}_t C) d\mathbf{p}' \right], \quad (1)$$

$$\dot{\mathbf{x}} = U_0 \mathbf{p} + \mathbf{u} - D \nabla_x (\ln \Psi), \quad (2)$$

$$\dot{\mathbf{p}} = (\mathbf{I} - \mathbf{p}\mathbf{p}^T)(\gamma \mathbf{E} + \mathbf{W})\mathbf{p} - d_r \nabla_p (\ln \Psi). \quad (3)$$

Equations (2) and (3) give the fluxes associated with swimmer position and orientation. The former encodes the features that a swimmer propels itself along its axis $\mathbf{p}$ with speed U_0 while also being carried along by the background flow $\mathbf{u}$. The last term allows for an isotropic translational diffusion with diffusion constant D. Equation (3) describes the rotation of an ellipsoidal particle by the local fluid flow, with $\mathbf{E} = (\nabla \mathbf{u} + \nabla^T \mathbf{u})/2$, $\mathbf{W} = (\nabla \mathbf{u} - \nabla^T \mathbf{u})/2$, and γ is a shape parameter $-1 \leqslant \gamma \leqslant 1$ [for an ellipsoidal particle with aspect ratio A, $\gamma = (A^2 - 1)/(A^2 + 1)$; for a sphere $\gamma = 0$ and for a slender rod $\gamma \approx 1$]. With $\nabla_\mathbf{p}$ the gradient operator on the sphere $|\mathbf{p}| = 1$, the last term models rotational diffusion of the swimmer with a diffusion constant d_r, as in Ref. [6].

Run-and-tumble chemotaxis is modeled by the terms in the second line of Eq. (1), where the first represents loss of swimmers tumbling from orientation $\mathbf{p}$ to other orientations and the second is a balancing source that accounts for swimmers tumbling from other orientations $\mathbf{p}'$ to $\mathbf{p}$. Here $\lambda(\mathcal{D}_t C)$ is the chemical gradient-dependent tumbling frequency, with $C(\mathbf{x}, t)$ the chemoattractant concentration. The tumbling frequency is related to the probability of a bacterium having a tumbling event within a fixed time interval. The total microswimmer population is taken to be constant, though cell division of chemotactic cells can also lead to intriguing dynamics [34].

From experiments [35], when the temporal rate-of-change of the chemoattractant concentration is positive along a swimmer's path, its tumbling rate reduces. If the chemoattractant concentration is constant or decreasing, then the tumbling rate is constant. Based on these studies [33], we model this response with a piecewise linear form:

$$\lambda(\mathcal{D}_t C) = \begin{cases} \lambda_0 (1 - \chi \mathcal{D}_t C) & \text{if } 0 < \mathcal{D}_t C < 1/\chi \\ 0 & \text{if } 1/\chi < \mathcal{D}_t C \\ \lambda_0 & \text{otherwise} \end{cases}, \quad (4)$$

$$\mathcal{D}_t C = \frac{\partial C}{\partial t} + (\mathbf{u} + U_0 \mathbf{p}) \cdot \nabla C, \quad (5)$$

is the rate-of-change of the chemoattractant concentration along the swimmer's path. The parameter λ_0 is the basal stopping rate or tumbling frequency in the absence of chemotaxis, whereas χ is the chemotactic strength. In the literature the frequency response λ has been approximated in various forms, exponential [33,36,37] or linearized [24], and most often does not include the temporal gradient [21], chemoattractant, or fluid dynamics. For ease of linear stability analysis, here we use only the linear form for the the frequency response, but note that the model and numerical simulations allow for any form suggested by the experiments.

Anisotropic tumbling can be included in the integral term in Eq. (1) via a "turning kernel" dependent on $|\mathbf{p} - \mathbf{p}'|$, where $\mathbf{p}$ and $\mathbf{p}'$ are pre- and posttumble directions [32,38]. Here we focus on isotropic tumbles only.

The fluid velocity $\mathbf{u}(\mathbf{x}, t)$ satisfies the Stokes equations with an active particle stress due to their motion in it,

$$-\nabla_x^2 \mathbf{u} + \nabla_x q = \nabla_x \cdot \Sigma^a, \quad \nabla_x \cdot \mathbf{u} = 0. \quad (6)$$

Here q the fluid pressure and Σ^a the active stress,

$$\Sigma^a(\mathbf{x}, t) = \alpha \int \Psi(\mathbf{x}, \mathbf{p}, t)(\mathbf{p}\mathbf{p}^T - \mathbf{I}/3)d\mathbf{p}. \qquad (7)$$

The active stress Σ^a is a configuration average over all orientations $\mathbf{p}$ of the stresslets $\alpha(\mathbf{p}\mathbf{p}^T - \mathbf{I}/3)$ exerted by the particles when moving in the fluid. The stresslet strength α is a $O(1)$ constant [6]. For *pushers*, swimmers like bacteria that propel themselves with rear-mounted flagella, $\alpha < 0$. For *pullers*, swimmers like microalga *Chlamydomonas reinhardtii* that propel with front flagella, $\alpha > 0$.

We define the local swimmer concentration $\Phi(\mathbf{x}, t)$ and mean swimmer director vector $< \mathbf{p}(\mathbf{x}, t) >$,

$$\Phi(\mathbf{x}, t) = \int \Psi(\mathbf{x}, \mathbf{p}, t)d\mathbf{p}, < \mathbf{p}(\mathbf{x}, t) > = \int \mathbf{p}\Psi(\mathbf{x}, \mathbf{p}, t)d\mathbf{p}.$$

The chemoattractant or nutrient is dispersed in the fluid and has a dynamics of its own that includes fluid advection and molecular diffusion. Similarly to the original KS model [19] but with fluid advection included, the chemoattractant evolves as

$$\frac{\partial C}{\partial t} + \mathbf{u} \cdot \boldsymbol{\nabla} C = D_c \nabla^2 C - \beta_1 C + \beta_2 \Phi, \qquad (8)$$

where D_c is the diffusion constant and $-\beta_1 C$ models chemoattractant degradation with a constant rate β_1, while $\beta_2 \Phi$ describes local production ($\beta_2 > 0$) or consumption ($\beta_2 < 0$) of chemoattractant by the swimmers. For ease of writing, we differentiate between the cases of *autochemotaxis* ($\beta_2 > 0$), where the swimmers themselves produce the chemoattractant, and when the swimmers respond to an externally supplied chemoattractant like a nutrient or oxygen ($\beta_2 \leqslant 0$). The focus of the analysis here is on autochemotaxis; the other type is investigated experimentally in Ref. [39] and theoretically in Refs. [32,36,37,40].

Taken together, the chemoattractant equation (8), the equation (1) for the probability distribution function Ψ (and hence Φ), and the Stokes equations (6) with active particle stress constitute a closed system that describes the dynamics of a motile suspension influenced by run-and-tumble autochemotaxis. We refer to this model as the *RT chemotaxis* model.

B. The turning-particle model

As an interesting alternative, we also consider a different chemotaxis model for suspensions of nontumbling microswimmers that can directly respond to a chemoattractant gradient. This turning model, while not applicable to bacteria whose chemotactic motion results from a modulation of runs and tumbles, is reminiscent of phoretic particles [41,42] that overall turn and migrate in the direction of the gradient of the chemical that fuels them. The suspension dynamics is described by

$$\frac{\partial \Psi}{\partial t} = -\boldsymbol{\nabla}_x \cdot [\Psi \dot{\mathbf{x}}] - \boldsymbol{\nabla}_p \cdot [\Psi \dot{\mathbf{p}}], \qquad (9)$$

$$\dot{\mathbf{x}} = U_0 \mathbf{p} + \mathbf{u} - D\boldsymbol{\nabla}_x(\ln \Psi), \qquad (10)$$

$$\dot{\mathbf{p}} = (\mathbf{I} - \mathbf{p}\mathbf{p}^T)[(\gamma \mathbf{E} + \mathbf{W})\mathbf{p} + \xi \boldsymbol{\nabla}_x C] - d_r \boldsymbol{\nabla}_p(\ln \Psi). \quad (11)$$

While there are no tumbling terms in Eq. (9), Eq. (11) now contains the term $\xi(\mathbf{I} - \mathbf{p}\mathbf{p}^T)\boldsymbol{\nabla} C$, which induces a "chemotactic" swimmer rotation towards the local direction of steepest ascent of the chemoattractant gradient. The constant ξ sets the timescale of this rotation. This rotation should be distinguished from rotational diffusion, which acts on very rapid timescales and is associated with very small changes in direction. Chemotaxis represented as a bias in the direction of individual swimming has often been used in numerical studies of active particles [43–47]. We impose a torque on the swimmers in Eq. (11) without accounting for the flow consequences which would be an antisymmetric active stress tensor in the fluid equations (6). This is justified since the leading-order flow singularity measured for bacteria and algae are a force dipole (decay as $1/r^2$ with distance r) not a torque monopole (also decay $1/r^2$) [48,49].

The chemoattractant equation (8), together with Eq. (9) for the probability distribution function Ψ and the Stokes equations (6) with active particle stress, constitute a closed system of equations that describe the dynamics of a chemotactic motile suspension with an evolving chemical field. We will refer to this set of equations as the *turning-particle (TP) chemotaxis* model.

C. A note on nondimensionalization

Equations (1)–(8) are shown in dimensionless form. The characteristic scales used for nondimensionalization are

$$\Psi_c = n, u_c = U_0, \ell_c = 1/n\ell^2, t_c = \ell_c/u_c, \qquad (12)$$

where $n = N/V$ is the mean number density of the swimmers, that is, the number of particles in a box domain with side L and volume $V = L^3$. Here U_0 is the intrinsic swimmer speed and ℓ the swimmer length. Since both our models follow the convention in Refs. [5,6], the rescaled system size L/ℓ_c encapsulates the swimmer concentration n, which may not be obvious from looking at Eqs. (1)–(8). This choice helps to decrease the number of parameters for analysis. We remark that $\ell_c = (V/V_p)\ell$, where $V_p = N\ell^3$ is the effective swimmer volume.

The dimensionless stresslet or force-dipole strength is $\alpha = \sigma_0/(U_0\mu\ell^2)$, where μ is the water viscosity and $\sigma_0(\mathbf{p}\mathbf{p}^T - \mathbf{I})$ is the stresslet generated by a swimmer with direction $\mathbf{p}$ [4–7,36,37].

Assuming a mean chemoattractant concentration scale C_c, other parameters are made nondimensional as

$$\lambda_0 = \tilde{\lambda}_0 t_c, \quad \chi = \tilde{\chi} C_c/t_c, \quad \xi = \tilde{\xi} C_c t_c/\ell_c$$
$$\beta_1 = \tilde{\beta}_1 t_c, \quad \beta_2 = \tilde{\beta}_2 n t_c/C_c, \qquad (13)$$

where $\tilde{\lambda}_0, \tilde{\chi}, \tilde{\xi}, \tilde{\beta}_1, \tilde{\beta}_2$ are the dimensional constants.

The nondimensional diffusion constants are

$$D = \tilde{D}t_c/\ell_c^2, \quad d_r = \tilde{d}_r t_c, \quad D_c = \tilde{D}_c t_c/\ell_c^2. \qquad (14)$$

These choices normalize the distribution function as

$$\frac{1}{V}\int_V d\mathbf{x} \int d\mathbf{p}\Psi(\mathbf{x}, \mathbf{p}, t) = 1 \qquad (15)$$

with $\Psi_0 = 1/4\pi$ the uniform isotropic state.

D. Estimating parameters from experiments

To help in comparisons with experiments, we discuss here how parameters measured in experiments can translate to our nondimensionless constants. While many types of microswimmers and chemoattractant types can be found in nature and in the laboratory, we illustrate the process for the case of swimming chemotactic bacteria *E. coli* for which many of these constants are either known or can be estimated.

Escherichia coli has length $\ell \approx 2$–$5\mu m$ and swims in water with speed $U_0 \approx 20$–$25\ \mu m/s$ and the strength of its force dipole has been measured in experiments as $\sigma_0 = 0.1$–1 pN [48]. Assuming water viscosity $\mu = 10^{-3}$ kg/ms, we obtain $\alpha \approx 0.1$–10, which is consistent with $O(1)$ used in prior simulation studies [5,6,31].

We assume a swimmer concentration $n = 5 \times 10^9/\text{cm}^3$ as in experiments with bacteria *Bacillus subtilis* [1,2]. This gives us characteristic scales $\ell_c = 50\ \mu$m and $t_c = 2s$ assuming $u_c = 25\ \mu$m.

Using data from the experiments of Saragosti *et al.* [25,26] with *E. coli*, we can approximate the other rate constants. They give basal a tumbling frequency of $\tilde{\lambda}_0 = 3\text{s}^{-1}$, mean chemoattractant concentration $C_c = 1.5 \times 10^{17}$ mol/cm^3, degradation rate $\tilde{\beta}_1 = 5 \times 10^{-3}$ mol s^{-1}, production rate $\tilde{\beta}_2 = 4 \times 10^5$ s^{-1} and the chemotactic strength can be extracted as $\tilde{\chi}/C_c = 4$. Using Eqs. (13) we obtain $\lambda_0 = 6$, $\beta_1 = 0.01$, $\beta_2 = 0.05$, and $\chi = 2$. Notice that $\chi\beta_2/\beta_1 = 10 > 1/6 = 1/\lambda_0$ so these parameters lie in the unstable regime predicted by the linear analysis.

Also from Refs. [25,26] we get $\tilde{D}_c \approx 5 \times 10^{-6}$ cm^2/s which gives us $D_c = 0.4$. Note that the Péclet number is then Pe $= 1/D_c \approx 2.5$. For faster-swimming organisms, such as marine bac0teria this intrinsic Péclet number can reach $O(10 - 20)$ [31].

We note that the estimated values above are of similar magnitude to those used in many theoretical studies.

III. STABILITY ANALYSIS

A. Linear stability of RT autochemotaxis

Analysis of the system linearized about the uniform isotropic state ($\Psi_0 = 1/4\pi$), with quasistatic chemoattractant field in the case of no swimmer diffusion ($D = 0 = d_r$) reveals two distinct dispersion relations,

$$1 = \frac{-3\alpha\gamma}{4ik}\left[2a_H^3 - \frac{4}{3}a_H + \left(a_H^4 - a_H^2\right)\log\frac{a_H - 1}{a_H + 1}\right], \quad (16)$$

$$1 = \frac{\lambda_0\chi}{2}R\left[2 + a_C\log\frac{a_C - 1}{a_C + 1}\right] - \frac{\lambda_0}{2}\frac{1}{ik}\log\frac{a_C - 1}{a_C + 1}, \quad (17)$$

where $a = (\sigma + \lambda_0)/ik$ and $R = \beta_2/(\beta_1 + k^2 D_c)$, with σ the growth rate and $k = |\mathbf{k}|$ the wave number. We refer to Eqs. (16) and (17) as the hydrodynamic and autochemotactic dispersion relations, respectively.

The relation (16) is the same as that found for purely tumbling nonchemotactic swimmers by Subramanian and Koch [4], while the autochemotactic relation in (17) was reported earlier in Ref. [31]. Note that chemotaxis enters the hydrodynamic relation (16) solely through stopping rate λ_0. The fluid dynamics and its effects (e.g., the swimming mechanism

typified by the parameter α) do not appear in the autochemotactic relation (17), but the quasistatic chemoattractant dynamics is included in the term $R = \beta_2/(\beta_1 + k^2 D_c)$.

From Eq. (16) we obtain two branches for $\sigma(k)$ in the small k (large system size) limit, namely

$$\sigma_{H1} \approx -\alpha\gamma/5 - \lambda_0 + 15/(7\alpha\gamma)k^2 + \dots,$$

$$\sigma_{H2} \approx -\lambda_0 - 1/(\alpha\gamma)k^2 + \dots. \quad (18)$$

The chemotactic relation Eq. (17) gives only one branch

$$\sigma_C \approx 1/(3\lambda_0)(\lambda_0\chi\beta_1/\beta_2 - 1)k^2 + \dots. \quad (19)$$

We solve the dispersion relations Eqs. (16) and (17) for $\sigma(k)$ numerically using Newton's method and the small-k asymptotic solutions as initial guesses (Fig. 1).

For pushers ($\alpha < 0$) there is a hydrodynamic instability for a finite band of wave numbers $k \in [0, k_c \approx 0.55)$. Tumbling diminishes this range of unstable wave numbers as the branch is brought down by λ_0 [while Im(σ_H) and the oscillatory modes remain unaffected]. Moreover, we can obtain a range of λ_0 for which a hydrodynamic instability is possible for pushers. We find that for $\lambda_0 \geqslant 0.2$ there can be no hydrodynamic instability for any system size or swimmer shape. For pullers, there is no hydrodynamic instability, as Re$[\sigma_H(k)] < 0$ even for $\lambda_0 = 0$.

For the autochemotactic dispersion relation, the long-wave asymptotics in Eq. (17), there are wave numbers k with Re$[\sigma_C(k)] > 0$ for pushers and pullers alike and for any swimmer shape parameter γ. Autochemotaxis thus introduces a new instability branch, which is solved numerically from Eq. (17) and plotted in Fig. 1(b) for two sets of λ_0, χ, D_c. Note that we can obtain a range of parameters for which there is a chemotactic instability ($\sigma_C > 0$ for $k > 0$); they have to satisfy $\chi\beta_2\lambda_0/\beta_1 > 1$.

B. Linear stability of TP autochemotaxis

The linear stability analysis of the TP model of is done in a similar manner, and the results obtained are remarkably similar to the RT model with linearized tumbling rate, even though there is no tumbling in this instance. For swimmers with no translational or rotational diffusion ($D = d_r = 0$), the two dispersion relations are

$$1 = \frac{-3\alpha\gamma}{4ik}\left[2a_H^3 - \frac{4}{3}a_H + \left(a_H^4 - a_H^2\right)\log\frac{a_H - 1}{a_H + 1}\right], \quad (20)$$

$$1 = \xi R\left[2 + a_C\log\frac{a_C - 1}{a_C + 1}\right], \quad (21)$$

with $a = -i\sigma/k$. The long-wave (small k) asymptotics for the hydrodynamics relation yields

$$\sigma_{H1} \approx -\frac{\alpha\gamma}{5} + \frac{15}{7\alpha\gamma}k^2 + \dots, \quad \sigma_{H2} \approx -\frac{1}{\alpha\gamma}k^2 + \dots, \quad (22)$$

which resemble the RT results without basal tumbling, Eqs. (18). The small-k asymptotics of the autochemotactic relation give

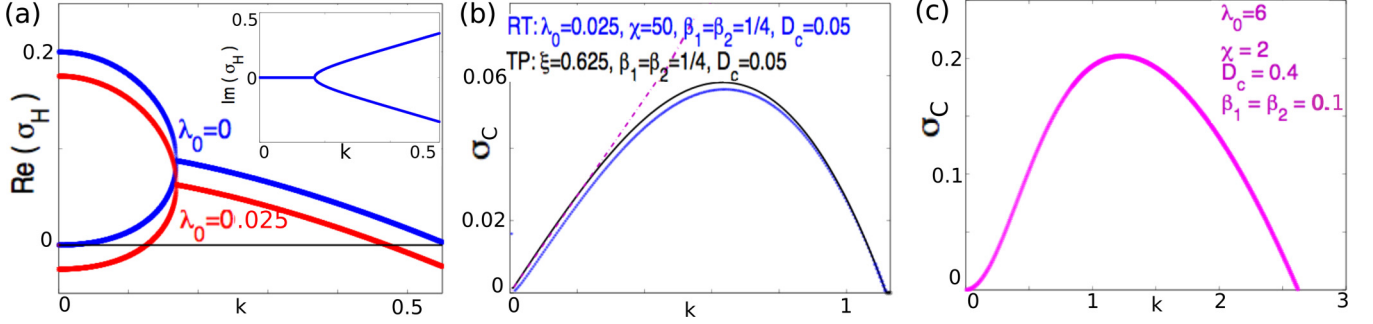$$\sigma_C \approx \sigma_1 k + \sigma_3 k^3 + \dots \quad (23)$$

FIG. 1. (a) The two branches of the growth rate obtained by the hydrodynamic relation with $\alpha = -1$, $\gamma = 1$. Inset shows the imaginary parts. (b) The growth rate obtained from the RT chemotaxis relation for $\lambda_0 = 0.025$, $\chi = 50$ used later for simulations. For both, $\beta_1 = \beta_2 = 1/4$, $D_c = 1/20$. Also shown is the growth rate from the TP relation: with $\xi = 5$ and $\xi = 0.625$ (inset) and $\beta_1 = \beta_2 = 1/4$, $D_c = 1/20$. Dashed line show the long-wave asymptotic result. Parameters ξ are chosen so that $\xi = \lambda_0 \chi / 2$. (c) The growth rate obtained from the RT chemotaxis relation for $\lambda_0 = 6$, $\chi = 2$, $D_c = 0.4$, $\beta_1 = \beta_2 = 0.1$ from the estimates in Sec. II D.

with $\sigma_1 \approx \xi[1 - \arctan(1)]\beta_2/\beta_1$ and $\sigma_3 \approx D_c/\beta_1$. While this does not look similar to the RT result Eq. (19), the numerical solution in Figs. 1(b) and 1(c) shows similarities in the overall curve shape, maxima, and critical k_c where $\sigma(k_c) = 0$. It can also be shown that the hydrodynamic instability increases growth of the shear stresses, whereas the autochemotactic instability increases fluctuations in the swimmer concentration and normal stresses [31,32,50].

Including translational diffusion merely shifts down the $\mathrm{Re}(\sigma_H)$ and $\mathrm{Re}(\sigma_C)$ by $-Dk^2$. As found in Ref. [51] for nonchemotactic swimmers, the hydrodynamic instability branch $\mathrm{Re}(\sigma_H)$ shifts down by approximately $6d_r$. Note that swimmer tumbling also shifts down the $\mathrm{Re}(\sigma_H)$ branches in Eqs. (18) by the basal frequency λ_0. We do not investigate here how nonzero rotational diffusion d_r affects the chemotactic instability.

C. Configurational entropy

The configurational entropy $\mathcal{S} = \iint \frac{\Psi}{\Psi_0} \log(\frac{\Psi}{\Psi_0}) d\mathbf{p} d\mathbf{x}$, with $\Psi_0 = 1/4\pi$, plays the role of a system energy [6]. Note that $\mathcal{S} \geqslant 0$ and realizes its minimum value of zero only for the homogenous and isotropic state Ψ_0. An increase in $\mathcal{S}$ means a departure from Ψ_0, e.g., through aggregation or alignment of swimmers.

For the TP model, it is possible to show that

$$4\pi \mathcal{S}_t^{TP} = 2\xi \int \Phi \mathbf{n} \cdot \nabla_x C d\mathbf{x} - \frac{6\gamma}{\alpha} \int \mathbf{E} : \mathbf{E} d\mathbf{x}$$
$$- \iint \Psi \big[D |\nabla_x \log \Psi|^2 + d_r |\nabla_p \log \Psi|^2 \big] d\mathbf{p} d\mathbf{x}.$$
(24)

The significance of the last two terms on the right-hand side is known for nonchemotactic swimmers. The second term includes the rate of the viscous dissipation and indicates a growth for suspensions of pushers ($\alpha = -1$) and decay for pullers ($\alpha = 1$) [6]. The last term indicates decay due to translational and rotational diffusion. The first term on the right-hand side implies growth due to a chemical gradient $\nabla_x C$ if the chemotactic sensitivity ξ is positive (i.e., the chemical is an attractant) for any type of swimmer of any shape. Specifically, if the swimmer flux $\Phi \mathbf{n}$ aligns in the chemoattractant

gradient direction $\nabla_x C$, then there is a positive contribution to the configurational entropy. The chemoattractant dynamics does not appear other than by its spatial gradient $\nabla_x C$.

Obtaining a similar equation for the full RT model is not easy, but for a system linearized around the uniform isotropic state $\Psi_0 = 1/4\pi$ it is possible to show that

$$4\pi \mathcal{S}_t^{\mathrm{RT}} = -\lambda_0 \mathcal{S}^{\mathrm{RT}} + \lambda_0 \chi \int \Phi \mathbf{n} \cdot \nabla_x C d\mathbf{x} - \frac{6\gamma}{\alpha} \int \mathbf{E} : \mathbf{E} d\mathbf{x}$$
$$- \iint \Psi \big[D |\nabla_x \log \Psi|^2 + d_r |\nabla_p \log \Psi|^2 \big] d\mathbf{p} d\mathbf{x}.$$
(25)

This equation shows the same last two terms as in Eq. (24) that are due to hydrodynamics and diffusion. The chemotactic term is also similar, except here it has the factor $\lambda_0 \chi$ instead of 2ξ. A new term $-\lambda_0 \mathcal{S}^{\mathrm{RT}}$ appears here indicating the stabilization due to tumbling.

D. Relating the two chemotaxis models

In the RT model tumbling stabilizes the system; the hydrodynamic instability branches are shifted downwards by the basal tumbling frequency λ_0, as seen in Fig. 1. Rotational diffusion shifts down the hydrodynamic instability branches in by approximately $6d_r$ as shown by Hohenegger and Shelley [51] for $k \ll 1$. In this respect, at large system sizes tumbling with basal frequency λ_0 acts like rotational diffusion with coefficient $6d_r$, as noted by other theoretical studies [4].

Comparing the chemotactic dispersion relations, Eqs. (17) and (21), and the configurational entropy results in Eqs. (24) and (25) suggests that $\xi \approx \lambda_0 \chi / 2$ relates the RT model with basal tumbling λ_0 and chemotactic strength χ to the TP chemotaxis model with strength ξ. Since in the $k \ll 1$ regime the chemotactic growth rate of the TP model is $\sigma_C \approx \xi[1 - \arctan(1)]\beta_2/\beta_1 k$, we plot the line with slope $\lambda_0 \chi / 2[1 - \arctan(1)]\beta_2/\beta_1$ in Fig. 1(b) and see that it gives a remarkable approximation to the growth rate from the RT model. Comparison of the curves in Figs. 1(b) and 1(c) for the RT and the TP models, when the chemotactic parameters are matched as such, shows also their similarity in overall curve shape, maxima, and critical wave numbers k_c where $\sigma(k_c) = 0$.

Thus, for $k \ll 1$ or large wavelengths, the linearized TP model with chemotactic parameter ξ and rotational diffusion d_r behaves similarly to the linearized RT model with basal tumbling λ_0 and chemotactic sensitivity χ, when the parameters are related as $\xi \approx \lambda_0 \chi / 2$ and $\lambda_0 = 6d_r$. Full nonlinear simulations with parameters chosen as above also support this matching, as is shown in the next section. Differences, however, may occur at small wavelengths or due to nonlinearities.

IV. NONLINEAR SIMULATIONS

For relative ease of computation, we perform simulations in two dimensions (2D) instead of 3D and modify the Eqs. (1)–(8) accordingly. We consider doubly periodic systems in which the particles are in the (x, y) plane with orientation $\mathbf{p} = (\cos\theta, \sin\theta, 0)$ parametrized by an angle $\theta \in [0, 2\pi)$. We use discrete Fourier transforms to approximate spatial derivatives and to solve the fluid equations (6). Integrations in θ to obtain the swimmer density Φ and active particle stresses Σ^a [Eq. (7)] use the trapezoidal rule. Equations (1) and (8) are integrated in time using a second-order scheme. Particle translational and rotational diffusion are included in all the simulations for numerical stability (with values of $D = d_r = 0.025$). We consider only slender rodlike microorganisms with shape parameter $\gamma = 1$ and pick the computational domain is a square with side $L = 50$ or $L = 25$. The initial swimmer distribution, used in all the examples, is taken to be a small perturbation about the uniform and isotropic state Ψ_0. The initial chemoattractant concentration is taken to be uniform and $C(\mathbf{x}, 0) = \beta_2/\beta_1$.

A. Effect of mixing dynamics on autochemotaxis of pusher suspensions

It is known that pusher suspensions ($\alpha < 0$) develop a hydrodynamic instability [4,6]. In that case (without chemotaxis or tumbling), that instability gives rise to strongly mixing flows with bands of high swimmer concentration [6]. We now illustrate the suspension dynamics when tumbling and chemotaxis are included.

We perform nonlinear simulations with $\lambda_0 = 0.025$, $\chi = 50$, $D_c = 1/20$, $\beta_1 = \beta_2 = 1/4$ in a square domain with side $L = 50$. For these parameters, the linear theory predicts dynamics with both strong autochemotactic and hydrodynamic instabilities. The parameters in this comparison are chosen to accentuate the differences in the results. For comparison we include the cases of purely tumbling suspensions ($\lambda_0 = 0.025$, $\chi = 0$), nonchemotactic suspension ($\lambda_0 = 0$), and another case for which linear analysis predicts just hydrodynamic, but no autochemotactic instability (with $\lambda_0 \chi \beta_2/\beta_1 < 1$).

Figure 2 shows plots of the swimmer concentration at the onset of the mixing regime. Chemotactic swimmers produce chemoattractant as well as aggregate towards it. A strongly mixing flow emerges and advects both swimmers and chemoattractant, resulting in *dynamic aggregation* of swimmers occurring due to the local autochemotactic tendency. This effect is seen from the sharper and narrower concentration bands in the autochemotactic suspension in Fig. 2(a) compared to nonchemotactic tumblers in Fig. 2(c).
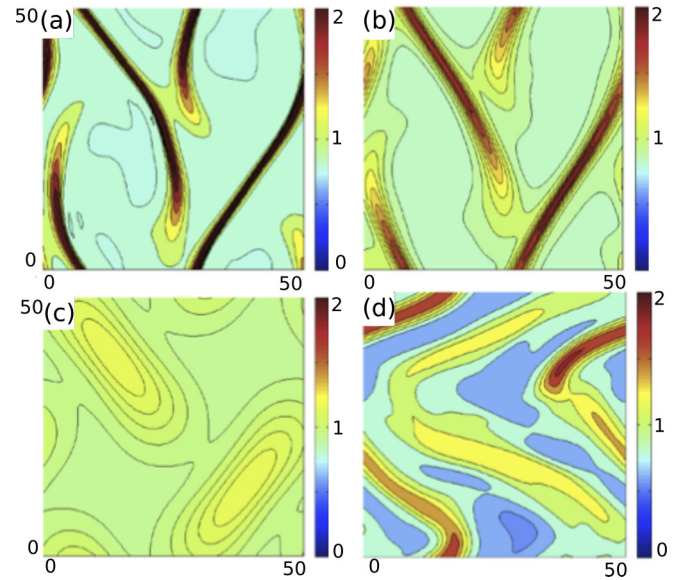

FIG. 2. RT chemotaxis model: Concentration Φ of pusher swimmers that are (a) strongly autochemotactic $\lambda_0 = 0.025$, $\chi = 50$, (b) weakly autochemotactic $\lambda_0 = 0.025$, $\chi = 35$ ($\lambda_0 \chi \beta_2/\beta_1 < 1$), (c) tumbling nonchemotactic $\lambda_0 = 0.025$, $\chi = 0$, (d) nontumbling $\lambda_0 = 0$, all at time $t = 150$.

Autochemotaxis stabilizes the formation of concentration bands that pure tumbling had diminished through its diffusion-like effect. The effect is apparent even for the case where no autochemotactic instability is predicted by linear theory ($\lambda_0 \chi \beta_2/\beta_1 < 1$), as shown in Fig. 2(b). In Figs. 2(a)–2(d) we see that autochemotaxis has also hastened the onset of the mixing regime when compared to the purely tumbling pusher suspension. Linear stability predicts that pure tumbling has a stabilizing effect on the suspension. This is confirmed in simulations when comparing the weak concentration bands
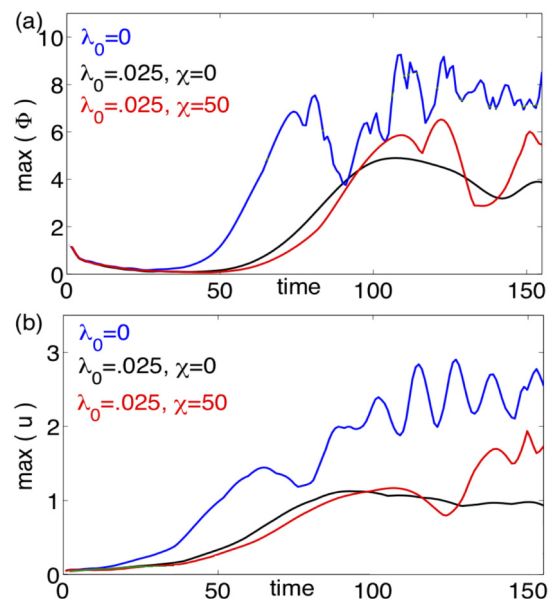

FIG. 3. RT chemotaxis model: (a) The maximum of the swimmer concentration Φ and (b) the maximum of the generated fluid flow $\mathbf{u}$ in Figs. 2(a), 2(c) and 2(d).
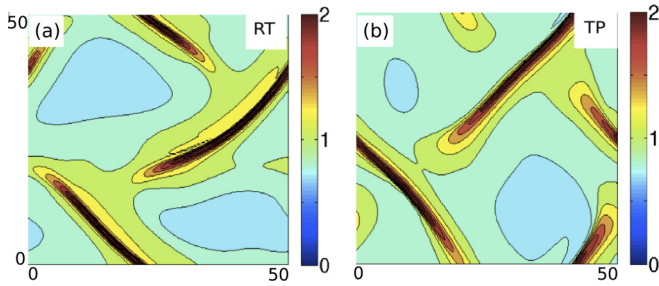
FIG. 4. Swimmer concentration Φ in pusher suspensions for the RT chemotaxis model with $\lambda_0 = 0.025$, $\chi = 60$, $d_r = 0.025$ (left) and TP chemotaxis model with $\xi = 0.75$, $d_r = 0.175$ (right) at time $t = 150$.

for pure-tumblers and the nontumbling nonchemotactic pushers in Figs. 2(c) and 2(d). These effects are also illustrated

in plots of the swimmer concentration and generated fluid flow in Fig. 3. Note from Fig. 3(b) that in pusher suspensions with the same tumbling frequency $\lambda_0 = 0.025$, autochemotaxis strengthens the emerging fluid flows. This suggests that autochemotaxis can be used to enhance mixing in pusher suspensions.

B. Similarities between the chemotaxis models

We illustrate the qualitative similarities in the dynamics of the two chemotaxis models when parameters are matched as suggested by the linear theory: $\lambda_0 \approx 6d_r$ and $\xi \approx \lambda_0 \chi / 2$. Figure 4 shows pusher swimmer concentration for the two models at the onset of mixing. The profiles and dynamics are remarkably similar, and similarity is observed in the chemoattractant field generated fluid flows (not shown). Similarity is
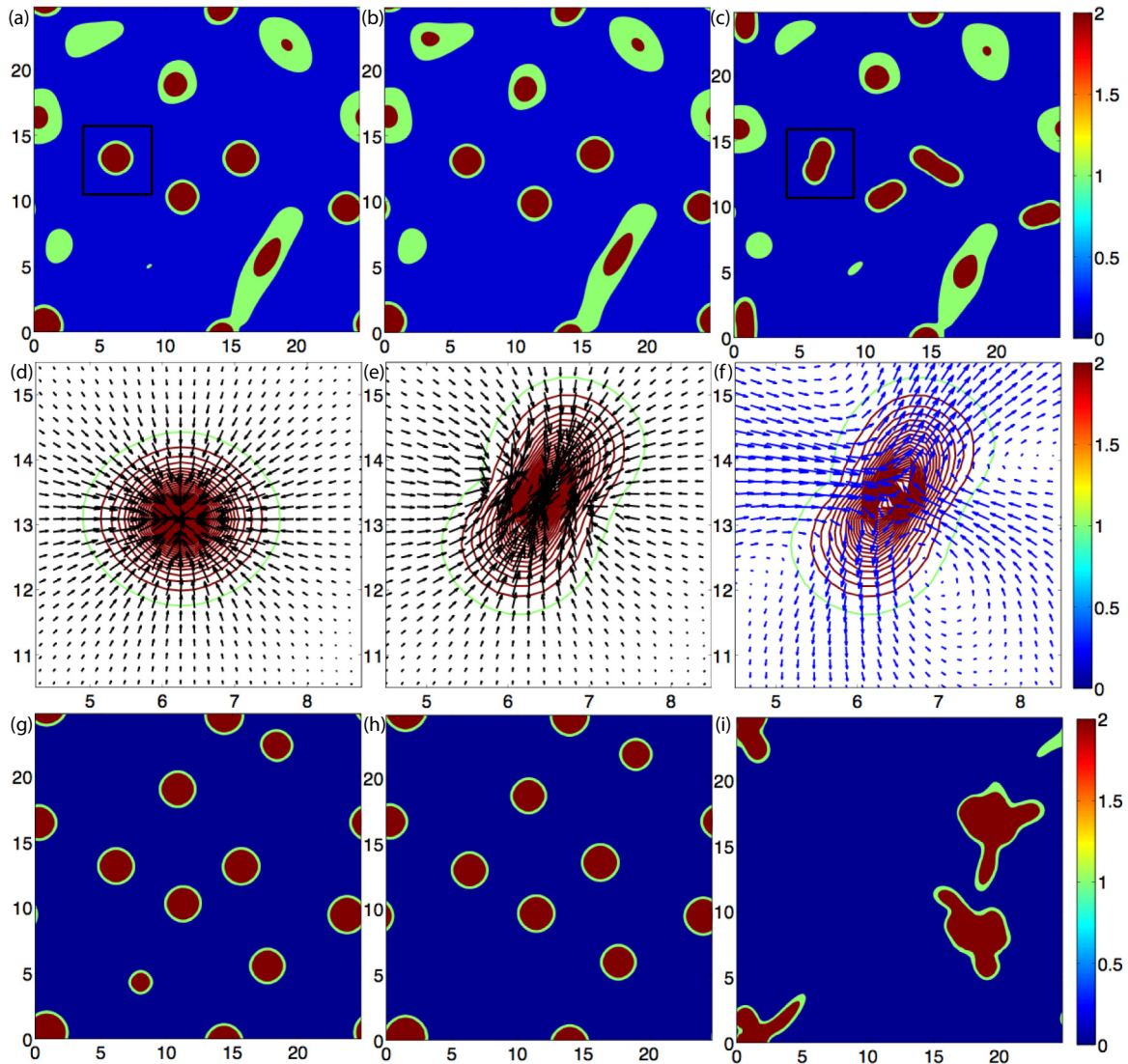

FIG. 5. Aggregation and clustering of autochemotactic microswimmers in the RT chemotaxis model. Displayed are the concentration Φ of (a) neutral, (b) puller, and (c) pusher swimmers at time $t = 50$. (d) Close-up of a peak in the puller suspensions showing concentration Φ level sets and mean swimmer direction $< \mathbf{p} >$. (e) Close-up of of a peak in the pusher suspension showing concentration Φ level sets and mean swimmer direction $< \mathbf{p} >$; in (f) the generated fluid flow $\mathbf{u}$. Panels (g), (h), and (i) show the concentration Φ of neutral, puller, and pusher swimmers at later time $t = 150$. See movies of the dynamics in Ref. [53].
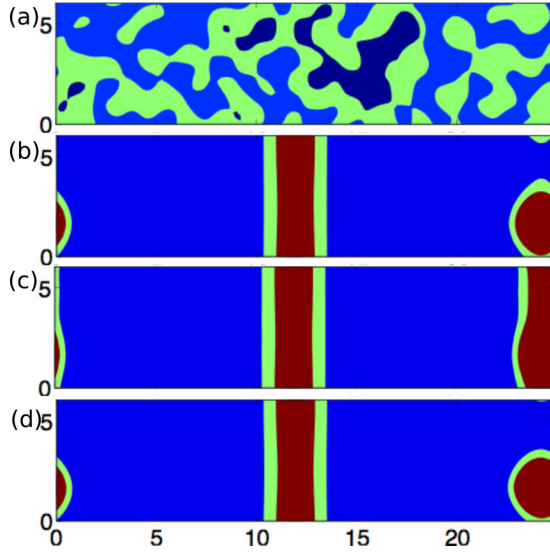
FIG. 6. The concentration field Φ in a channel with width $6.25 > L^s = 3$ at times (a) $t = 0$ and $t = 300$ for (b) neutral, (c) puller, and (d) pusher swimmers.

observed in simulations with pullers and neutral swimmers as well.

The TP model assumes that a swimmer is able to detect the local chemoattractant gradient and adjust its orientation to swim towards the regions of high chemoattractant concentration. This chemotactic response is induced through a torque that aligns the swimmers with the chemoattractant gradient. While not applicable to bacteria, it is intriguing that there are similarities to the RT chemotaxis model in the linear analysis and the also the nonlinear dynamics at the long wavelengths.

C. Clusters and squiggling aggregates

We perform simulations with parameters estimated from experiments (Sec. II D) $\lambda_0 = 6$, $\chi = 2$, $D_c = 0.4$, and we pick $\beta_1 = \beta_2 = 0.1$ and square domain side $L = 25$. The results are shown in Fig. 5. For these parameters, linear stability predicts chemotactic aggregation [see in Fig. 1(c) the plot of the growth rate] but no hydrodynamic instability for pushers since $\lambda_0 > 0.2$.

All three cases—neutral, puller, and pusher—begin from identical initial data that is a perturbation about uniform isotropy. As seen in Figs. 5(a) and 5(b), both the neutral swimmer and the puller suspensions stabilize into nearly identical patterns. This is not surprising since at these parameters, hydrodynamics is suppressed for puller suspensions. The aggregates are circular and saturated in magnitude. Conversely, the pusher suspension initially aggregates in the same locations, but the aggregates are now ellipsoidal [Fig. 5(c)] and are slowly squiggling as is suggested by the mean director field [Fig. 5(e)]. The underlying mechanism for the motion of the aggregates has to do with the local fluid flows generated in pusher suspensions, which though small, are present in regions of high swimmer concentration. The beanlike aggregate shapes seem to be due to the local straining flows at the local concentration peaks, and the shape is consistent with the direction of strain, as shown in Fig. 5(f).
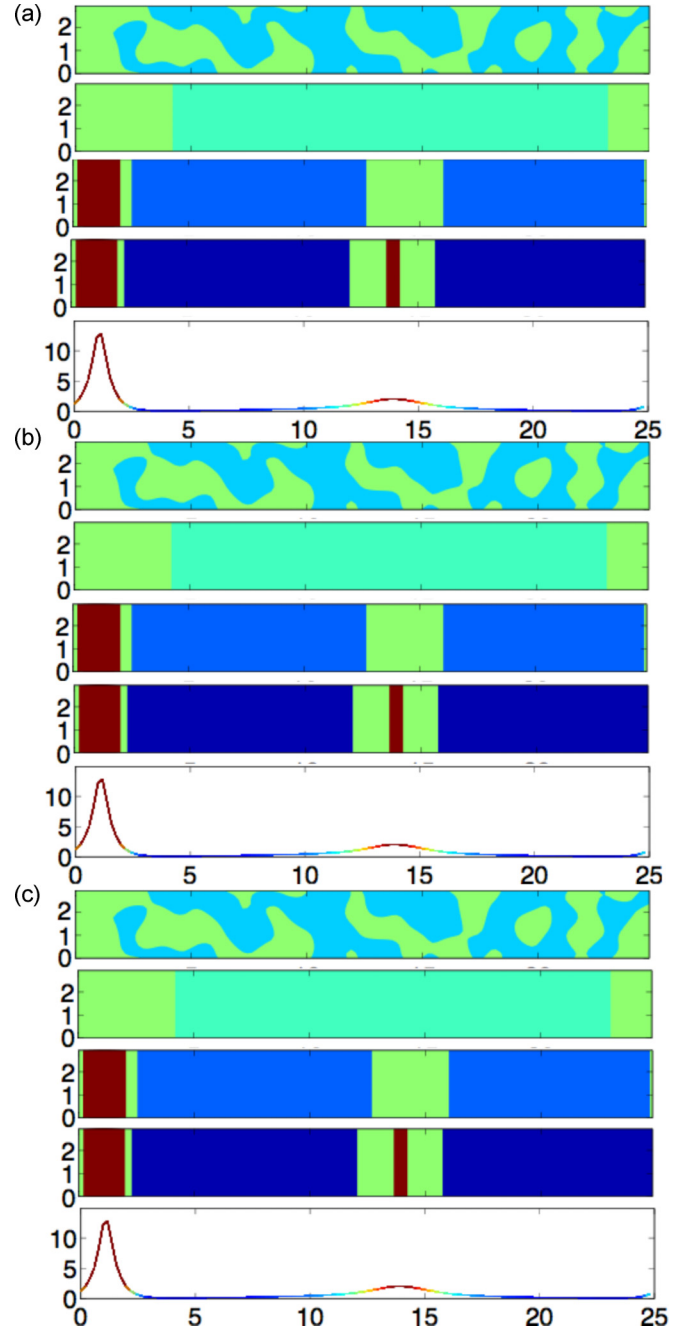

FIG. 7. The concentration field Φ in a channel with width $3.125 < L^s = 5.5$ at times $t = 0, 100, 200, 300$ for (a) neutral, (b) puller, and (c) pusher swimmers. The profiles (side-views) of Φ are shown at time $t = 300$. See the movie in Ref. [53].

In later times the neutral and puller aggregates remain stable circular aggregates, though the number of peaks may not be identical due to occasional merging of the peaks. The puller suspension has more peaks, and as explained in our prior study, this is likely due to the nontrivial straining fluid flows between peaks that keep them from further merging. In the pusher suspension though the initially elongated peaks squiggle and merge with each-other and occasionally break. The aggregate shape is asymmetric and continually changing.

TABLE I. Length scale of aggregates L^s measured in simulations for chemotactic parameters (λ_0, χ). We note with Y/N whether the patterns become quasi-1D in domains with one side 50 and the other side $\frac{50}{4} = 12.5$, $\frac{50}{8} = 6.25$, or $\frac{50}{16} = 3.125$.

(λ_0, χ)	(1,2)	(1,4)	$(\frac{1}{2},4)$	$(\frac{1}{2},8)$	$(\frac{1}{4},8)$	$(\frac{1}{4},16)$	$(\frac{1}{8},16)$
L^s	5.5	6.2	5.5	9.4	5.1	12	5.5
12.5	N	N	N	N	N	N	N
6.25	N	N	N	Y	N	Y	N
3.125	Y	Y	Y	Y	Y	Y	Y

These asymmetric and moving aggregates seem related to the filamentary aggregates reported in our previous study [31]. The pusher suspensions there were found to aggregate in long filaments that were slowly moving and squiggling; they would merge and break in a dynamic fashion but their characteristic width would remain unchanged. The beanlike aggregates seen in Fig. 5(c) and later time aggregates in Fig. 5(i) are a simpler version of the more complex dynamic structure reported in Ref. [31].

Note that in most cases of Fig. 5 the aggregates exhibit a characteristic size $L^s \approx 3$ where $L = 25$ is the domain size. The characteristic size L^s here is defined to be the mean length between isolines (contour lines) of the swimmer concentration with mean value $\overline{\Phi} = 1$, i.e., we measure the size of the aggregates from where their height surpasses the suspension mean concentration.

D. Stabilizing suspensions into concentration bands

Simulations shown previously reveal a length scale associated with the aggregates of all swimmer types. We conduct simulations in thin rectangular domains where the thin side is greater or smaller than this critical length scale L^s with otherwise the same parameters as in Fig. 5. Having one short domain direction mimics the thin microchannels used for experiments [26,52].

In domains with one side much larger than this critical length scale ($6.25 > L^s = 3$), the initially uniform and isotropic pusher suspension stabilizes into bean-shaped squiggling aggregates, as seen in Fig. 6. These aggregates are of similar size as those seen in the wider box-shaped domains of Fig. 5. Here the channel width is just above the critical length scale L^s, and the aggregate shapes oscillate between beanlike and bands.

In an even narrower domain with one side below the critical length ($3.125 < L^s = 5.5$), the pusher suspension now stabilizes instead into steady nearly one-dimensional bands, as seen in Fig. 7. These bands exhibit slow squiggling motion but are stable and do not further merge.

We explored this phenomenon for a variety of chemotactic parameters shown in Table I. Simulations in a rectangular domain with one side under this critical length scale L^s always show a transition into quasi-1D patterns.

E. Traveling concentration bands

Many experiments with autochemotactic bacteria have been performed in confined experimental setups such as
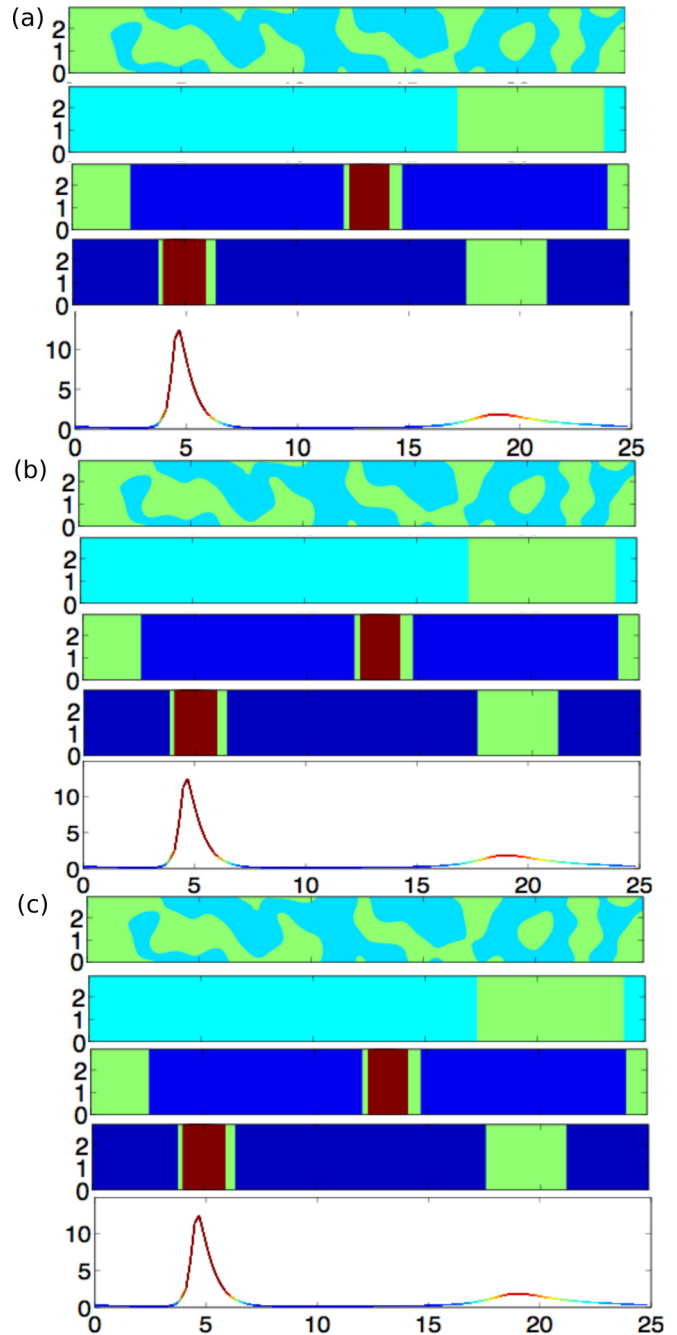

FIG. 8. The concentration field Φ under an imposed chemoattractant gradient in a channel with width $3.125 < L^s = 5.5$ at times $t = 0, 100, 200, 300$ for (a) neutral, (b) puller, and (c) pusher swimmers. The profiles (side views) of the concentration field are shown at time $t = 300$. See the movie of the dynamics in Ref. [53].

microchannels, with an imposed external chemoattractant [26] or temperature gradient [52]. Theoretical studies predicted that applied chemoattractant gradients affect hydrodynamic instabilities in pusher suspensions [54]. In experiments [25,26,52], the formation and propagation of one-dimensional concentration waves was observed. Autochemotactic aggregation seems to be a key ingredient in the production of traveling concentration pulses with the external chemoattractant or temperature gradient guiding them.
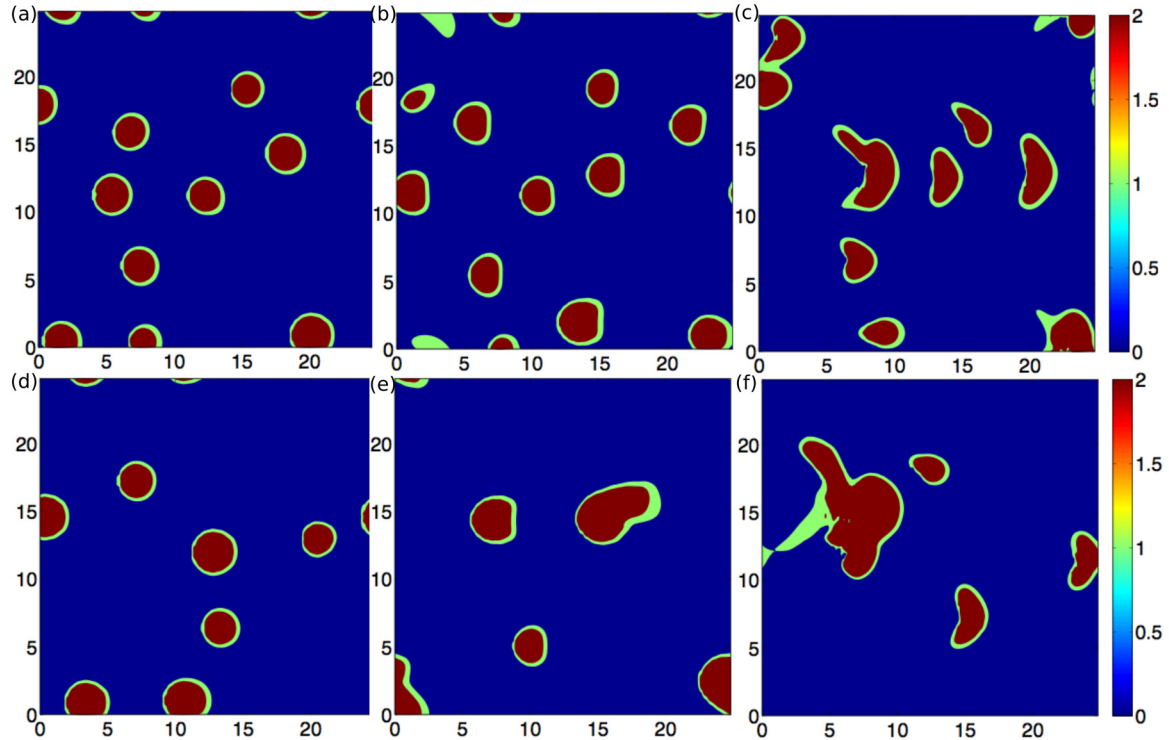
FIG. 9. Aggregation of autochemotactic microswimmers in the RT chemotaxis model when subjected to an external chemoattractant gradient with $\lambda_0 = 6$, $\chi^E = 6$. Displayed are the concentration Φ of (a) neutral, (b) puller, and (c) pusher swimmers at time $t = 50$. Panels (d), (e), and (f) show the concentration Φ of neutral, puller, and pusher swimmers at time $t = 150$. See movies in Ref. [53].

We explore this phenomenon by introducing a constant chemoattractant gradient along the channel, in addition to the intrinsically produced chemoattractant field. To do this, we include another term, $\mathcal{D}_t C^E$, in Eq. (4) with constant $\nabla C^E = [1, 0]$ and chemotactic parameters $\lambda_0^E = 6$, $\chi^E = 6$ which are consistent with the parameters in the experiments with chemotactic bacteria [25,26,52]. Note that such an implementation of the external gradient assumes it to be constant and does not account the stirring of the imposed attractant by the swimmers. The initial suspension is uniform and isotropic, with a uniform intrinsically produced chemoattractant ($C = \beta_2/\beta_1$). The results are shown in Fig. 8.

The short-term dynamics is dominated by autochemotactic aggregation into quasi-one-dimensional bands, Fig. 8(b). However, under the influence of the external gradient, these aggregate bands now propagate and interact with each other. Merging of the existing bands is observed, as are the birth and propagation of new ones; though the aggregates do not necessarily merge into one superband. Here the profiles are visibly asymmetric (compare to the case of no external gradient in Fig. 7). The profiles have a protruding front from which smaller bands may later emerge and break-off—a phenomenon observed in experiments with chemotactic bacteria, e.g., compare to Fig. 1 of Saragosti *et al.* [25].

F. Unconfined traveling aggregates

We saw in Fig. 5 that in unconfined spaces the chemotactic aggregates for neutral and puller swimmers are circular and nearly identical, whereas the pusher swimmer aggregates or

droplets squiggle and move due to the hydrodynamic interactions.

We impose an external chemoattractant gradient to an initially isotropic suspensions of swimmers and show the results in Fig. 9. The parameters used are the ones extracted from experiments in Ref. [26] and discussed in Sec. II D. The swimmers cluster and travel in group in the direction of the gradient. The aggregates of the neutral and puller swimmers are no longer similar, and the imposition of the external gradient highlights the differences. The puller swimmer aggregates in Figs. 9(b) and 9(e) are semicircular with the flat face facing the external gradient. The pusher swimmer aggregates [Fig. 9(c)] are mostly sickle shaped and the convex part faces the gradient. In the later times, the aggregates for all the swimmer types may have merged into larger aggregates. The external gradient helped the coarsening and merging of aggregates. For pullers and pushers hydrodynamics has further helped the merging process since there's fewer active droplets than in neutral swimmer case.

V. DISCUSSION AND CONCLUSION

We have presented and elaborated upon two kinetic models that couple chemoattractant production and response in colonies of microswimmers with the fluid flows that the swimmers generate while moving. These two models, and our study of them, merge together two separate areas of investigation: chemotactic aggregation due to population-produced chemoattractants and the hydrodynamics of active motile suspensions.

We performed the linear stability analysis and entropy analysis for both the models and find two distinct sources of instability: the chemotaxis-induced one which exhibits itself as an aggregation of swimmers and a hydrodynamic one in "pushers" that exhibits itself with local swimming alignment and the generation of nontrivial fluid flows. In the long-wave regime we see qualitative agreement between the two models when the parameters are matched as analysis predicts. We found that while tumbling by itself dampens the pusher collective dynamics, autochemotaxis can be used to revive it. This suggests chemotactic bacteria can achieve a more accelerated collective dynamics than nonchemotactic ones.

In our first study [31] we investigated the RT model using parameters close enough to those in the the Saragosti *et al.* experiments [26] and found the production of filamentary squiggly aggregates. Despite this system being well outside of the regime of hydrodynamic instability predicted by linear analysis, hydrodynamics was plainly important in their local dynamics. We explain here the emergence of those complex structures. In a setting of a narrow domain that mimics the microfluidic thin channels, these aggregates can become quasi-one-dimensional bands. These bands transition into one-dimensional traveling pulses when an external chemoattractant gradient is applied, and the results strongly resemble those observed in experiments with autochemotactic *E. coli* confined in microfluidic channels [26,52]. By mimicking the channel confinement with a narrow rectangular domain, our model qualitatively captures the traveling pulses. While most experiments are done in narrow microchannels, our simulations predict that in wide channels or unconfined spaces the traveling band or pulse phenomenon would exhibit itself as asymmetric squiggling aggregates that propagate in the direction of the imposed gradient.

We note that in our simulations here do not resolve the direct or hydrodynamic swimmer interactions with a solid boundary. It has recently been found that those mechanical interactions alone can lead to unidirectional motion of dense suspensions of bacteria along narrow microchannels or racetracks even in the absence of autochemotaxis or external gradients [55,56]. The full coupling of all mechanical and chemical interactions undoubtedly would yield rich behavior yet to be explored, whether theoretically or experimentally.

Our models use a dilute to semidilute theory that does not include local interactions between swimmers, either lubrication or steric; see Refs. [3,12,13,55,56] for relevant experiments using bacteria. In denser suspensions the swimmer size limits local swimmer density through steric interactions, and

well-founded models that combine these with hydrodynamic interactions are being developed [57]. We note a recent study by Taktikos *et al.* [45] for discrete disk-shaped chemotactic random walkers in 2D with steric but no hydrodynamic effects showing that steric interactions can limit aggregation, as indeed they must. Further, in dense suspensions it is not clear how run-and-tumble dynamics, as it is typically modeled, is affected by crowding and steric interactions. Intuitively, one expects the swimmer tumbling frequency to decrease in denser suspensions where mobility is limited due to crowding. Moreover, the particle swimming speed is not necessarily constant and may depend on the local swimmer density, which can also lead to fascinating patterns [58].

The coupling of autochemotaxis with collectively generated flows has not yet been systematically studied in an experimental setting. Chemotaxis in bacterial colonies has been previously exploited for enhancing mixing in microfluidic devices [59], but it has not yet been studied experimentally how such mixing is affected by autochemotaxis. With the recent possibility of specific engineering and tuning of the locomotion, tumbling and chemosensing in microswimmers [17], it might become possible to optimize mixing and transport of materials at the microscale. Moreover, the interplay among locomotion, fluid flows, chemotaxis, and quorum sensing can be further illuminated through the controlled introduction of exogenous chemoattractants [60]. Notably, chemotactic-like behavior is also observed in suspensions of synthetic microswimmers that exist in microfluidic environments (e.g., see Ref. [61] for experiments and Ref. [42] for theory). Such chemotactic responses might be exploited in the future in technological applications [61–68].

[1] C. Dombrowski, L. Cisneros, S. Chatkaew, R. E. Goldstein, and J. O. Kessler, Phys. Rev. Lett. **93**, 098103 (2004).

[2] L. Cisneros, R. Cortez, C. Dombrowski, R. E. Goldstein, and J. O. Kessler, Exp. Fluids **43**, 737 (2007).

[3] L. H. Cisneros, J. O. Kessler, S. Ganguly, and R. E. Goldstein, Phys. Rev. E **83**, 061907 (2011).

[4] G. Subramanian and D. L. Koch, J. Fluid Mech. **632**, 359 (2009).

[5] D. Saintillan and M. J. Shelley, Phys. Rev. Lett. **100**, 178103 (2008).

[6] D. Saintillan and M. J. Shelley, Phys. Fluids **20**, 123304 (2008).

[7] D. L. Koch and G. Subramanian, Ann. Rev. Fluid Mech. **43**, 637-59 (2011).

[8] D. Saintillan and M. J. Shelley, C. R. Phys. **14**, 497-517 (2013).

[9] M. Ardre, H. Henry, C. Douarche, and M. Plapp, Phys. Bio. **12**, 066015 (2015).

[10] J. Stenhammar, C. Nardini, R. W. Nash, D. Marenduzzo, and A. Morozov, Phys. Rev. Lett. **119**, 028005 (2017).

[11] N. Desai and A. M. Ardekani, Soft Matter **13**, 6033 (2017).

[12] J. Dunkel, S. Heidenreich, K. Drescher, H. H. Wensink, M. Bar, and R. E. Goldstein, Phys. Rev. Lett. **110**, 228102 (2013).

[13] A. Sokolov and I. S. Aranson, Phys. Rev. Lett. **109**, 248109 (2012).

[14] E. O. Budrene and H. C. Berg, Nature **349**, 630 (1991).

[15] E. O. Budrene and H. C. Berg, Nature **376**, 49 (2002).

[16] B. L. Bassler, Cell **109**, 421 (2002).

[17] S. Park, P. M. Wolanin, E. A. Yuzbashyan, P. Silberzan, J. B. Stock, and R. H. Austin, Science **301**, 188 (2003).

[18] E. F. Keller and L. A. Segel, J. Theor. Biol. **26**, 399 (1970).

[19] E. F. Keller and L. A. Segel, J. Theor. Biol. **30**, 225 (1971).

[20] S. Childress, Lect. Notes Biomath. Springer, Berlin, **55**, 61 (1984).

[21] M. J. Tindall, P. K. Maini, S. L. Porter, and J. P. Armitage, Bull. Math. Biophys. **70**, 1570 (2008).

[22] W. Alt, J. Math. Biol. **9**, 147 (1980).

[23] M. J. Schnitzer, Phys. Rev. E **48**, 2553 (1993).

[24] R. N. Bearon and T. J. Pedley, Bull. Math. Biophys. **62**, 775 (2000).

[25] J. Saragosti, V. Calvez, N. Bournaveas, A. Buguin, P. Silberzan, and B. Perthame, PLoS Comput. Biol. **10**, e1000890 (2010).

[26] J. Saragosti, V. Calvez, N. Bournaveas, B. Perthame, A. Buguin, and P. Silberzan, Proc. Natl. Acad. Sci. U.S.A. **108**, 16235 (2011).

[27] R. N. Bearon and A. L. Hazel, J. Fluid Mech. **771**, R3 (2015).

[28] B. Perthame, M. Tang, and N. Vauchelet, J. Math. Biol. **73**, 1161 (2016).

[29] H. C. Berg and D. A. Brown, Nature **239**, 500 (1972).

[30] H. C. Berg, *Random Walks in Biology*, expanded ed. (Princeton University Press, Princeton, NJ, 1993).

[31] E. Lushi, R. E. Goldstein, and M. J. Shelley, Phys. Rev. E **86**, 040902(R) (2012).

[32] E. Lushi, Ph.D. dissertation, New York University, 2011.

[33] K. C. Chen, R. M. Ford, and P. T. Cummings, J. Math. Biol. **47**, 518 (2003).

[34] A. Gelimson and R. Golestanian, Phys. Rev. Lett. **114**, 028101 (2015).

[35] R. M. Macnab and D. E. Koshland, Proc. Natl. Acad. Sci. U.S.A. **69**, 2509 (1972).

[36] T. V. Kasyap and D. L. Koch, Phys. Rev. Lett. **108**, 038101 (2012).

[37] T. V. Kasyap and D. L. Koch, J. Fluid Mech. **741**, 619 (2014).

[38] E. Lushi, Phys. Rev. E **94**, 022414 (2016).

[39] A. Sokolov, R. E. Goldstein, F. I. Feldchtein, and I. S. Aranson, Phys. Rev. E **80**, 031903 (2009).

[40] B. Ezhilan, A. A. Pahlavan, and D. Saintillan, Phys. Fluids **24**, 091701 (2012).

[41] J. L. Anderson, Annu. Rev. Fluid Mech. **21**, 61 (1989).

[42] S. Saha, R. Golestanian, and S. Ramaswamy, Phys. Rev. E **89**, 062316 (2014).

[43] R. Dillon, L. Fauci, and D. Gaver, J. Theor. Biol. **177**, 325 (1995).

[44] M. M. Hopkins and L. J. Fauci, J. Fluid Mech. **455**, 149 (2002).

[45] J. Taktikos, V. Zaburdaev, and H. Stark, Phys. Rev. E **85**, 051901 (2012).

[46] O. Pohl and H. Stark, Phys. Rev. Lett. **112**, 238303 (2014).

[47] E. J. Marsden, C. Valeriani, I. Sullivan, M. E. Cates, and D. Marenduzzo, Soft Matter **10**, 157-165 (2014).

[48] K. Drescher, J. Dunkel, L. H. Cisneros, S. Ganguly, and R. E. Goldstein, Proc. Natl. Acad. Sci. U.S.A. **108**, 10940 (2011).

[49] S. E. Spagnolie and E. Lauga, J. Fluid. Mech. **700**, 105 (2012).

[50] E. Lushi, R. E. Goldstein, and M. J. Shelley, arXiv:1310.7614 (2013).

[51] C. Hohenegger and M. J. Shelley, Phys. Rev. E **81**, 046311 (2010).

[52] H. Salman, A. Zilman, C. Loverdo, M. Jeffroy, and A. Libchaber, Phys. Rev. Lett. **97**, 118101 (2006).

[53] See Supplemental Material at http://link.aps.org/supplemental/10.1103/PhysRevE.98.052411 for movies showing the dynamics of pushers in elongated domains.

[54] G. Subramanian, D. L. Koch, and S. R. Fitzgibbon, Phys. Fluids **23**, 041901 (2011).

[55] H. Wioland, E. Lushi, and R. E. Goldstein, New J. Phys. **18**, 075002 (2016).

[56] E. Lushi, H. Wioland, and R. E. Goldstein, Proc. Natl. Acad. Sci. U.S.A. **111**, 9733 (2014).

[57] B. Ezhilan, M. J. Shelley, and D. Saintillan, Phys. Fluids **25**, 70607 (2013).

[58] X. Yang, D. Marenduzzo, and M. C. Marchetti, Phys. Rev. E **89**, 012711 (2014).

[59] M. J. Kim and K. S. Breuer, Anal. Chem. **79**, 955 (2007).

[60] C. Liu, X. Fu, L. Liu, X. Ren, C. K. L. Chau, S. Li, L. Xiang, H. Zeng, G. Chen, L.-H. Tang, P. Lenz, X. Cui, W. Huang, T. Hwa, and J.-D. Huang, Science **334**, 238 (2011).

[61] Y. Hong, N. M. K. Blackman, N. D. Kopp, A. Sen, and D. Velegol, Phys. Rev. Lett. **99**, 178103 (2007).

[62] A. Sen, M. Ibele, Y. Hong, and D. Velegol, Farad. Discuss. **143**, 15-27 (2009).

[63] D. Kagan, R. Laocharoensuk, M. Zimmerman, C. Clawson, S. Balasubramanian, D. Bishop, S. Sattayasamitsathit, L. Zhang, and J. Wang, Small **6**, 2741 (2010).

[64] S. Sundararajan, S. Sengupta, M. Ibele, and A. Sen, Small **6**, 1479 (2010).

[65] I. Theurkauff, C. Cottin-Bizonne, J. Palacci, C. Ybert, and L. Bocquet, Phys. Rev. Lett. **108**, 268303 (2012).

[66] W. Wang, W. Duan, A. Sen, and T. E. Mallouk, Proc. Natl. Acad. Sci. U.S.A. **110**, 17744 (2013).

[67] W. Wang, W. Duan, S. Ahmed, A. Sen, and T. E. Mallouk, Acc. Chem. Res. **48**, 1938 (2015).

[68] B. Liebchen and H. Lowen, Acc. Chem. Res. (2018), doi: 10.1021/acs.accounts.8b00215.